# Photolithography in Integrated Circuit Mask Metrology

Abstract: Photoresist technology is shown to have important advantages over the use of high-resolution silver halide films in dimensional metrology for integrated circuit masks. Experimental techniques are shown for the use of photoresist and chrome images in the study of image quality and uniformity and in analysis of the causes of image degradation. This method is applied to in situ lens evaluation and to the measurement of the precision of photorepeater stepping tables used in mask fabrication. In addition, the value of  $0.3 \mu m$  is established as the practical limit of dimensional tolerance in the present photolithographic technology, and its significance to the advancement of the state of the art in mask manufacture is discussed.

#### Introduction

New methods of measurement and analysis are required to meet the increasing needs of dimensional registration of masks in the various steps of integrated circuit manufacturing.

Generally, pattern fabrication starts with 10× masks, which are made by computer-controlled artwork generators. From these patterns are produced arrays of images by photoreduction with a step-and-repeat camera. The resulting 1× masks are then transferred to patterns on the wafer by means of contact exposure or 1:1 projection exposure in combination with photochemical processing.

The permissible dimensional registration tolerances between individual members of a mask set become more critical as the component densities are increased. There are two reasons for the difficulty in meeting tolerances: First, it is difficult to make the measurement system ten times more precise than the tolerance range being measured; and second, the individual causes of dimensional errors frequently are not known. This paper applies the resist technology technique to a variety of dimensional measuring tasks. Dimensional errors introduced by the projection lens and the stepping system are discussed as examples.

Experimental and theoretical aspects of lens characterization are reported in numerous papers. Particularly during the past two decades, introduction of Fourier

methods [1] and computer-aided design [2] have led to the fabrication of lenses having superior reproduction capabilities. However, the techniques for testing these lenses have lagged behind the advances in lens design. For instance, interlaboratory comparison of modulation transfer function (MTF) measurements by Hopkins and Dutton [3] show rms deviations in the order of 0.1 MTF units. Although transfer functions are useful to the lens designer, they have little correlation with the severe requirements that characterize these lenses. Thus the experimental evaluation of diffraction-limited, high-resolution lenses has returned full circle to evaluation by test images. Most authors who discuss test targets [4-9] use silver halide emulsions as the recording medium, which limits adequate evaluation. Photographic emulsions suffer from the following disadvantages in regard to dimensional metrology: They are at least five times thicker than resists and have an inherent granularity that limits resolution. Moreover, images cannot be added to halide emulsions after development, and the observation of the surface relief is difficult at high magnification. These limiting factors do not apply to photoresists [10].

Lens distortion has been measured by a number of authors [11-14] using silver halide emulsion. Photoresist technology, however, permits a more adequate measurement of the distortion in the submicron range, as is indicated in the section on lens evaluation. Another advan-

225

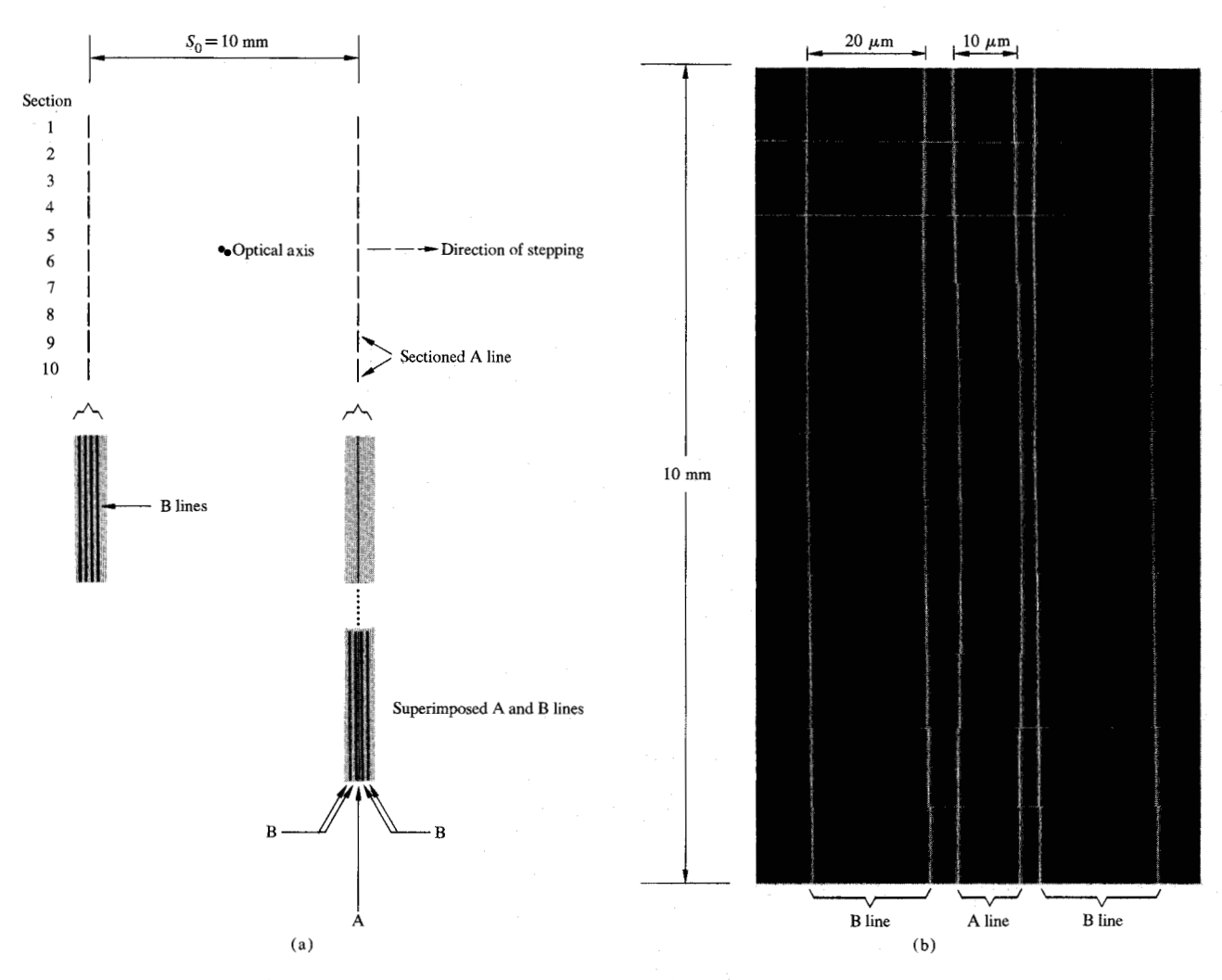


Figure 1 Measurement of lens distortion by use of a special test mask. (a) Arrangement of the parallel test lines at opposite sides of the 10-mm square field in the image plane. Step-and-repeat exposure at a  $\approx$  10 mm interval causes superposition of the B lines on the A line; (b) After processing, the final chrome lines are photographed in dark-field illumination at 1000×, whereby the sectioning of the lines permits convenient sampling at equidistant spots. The segments then are assembled such that the B lines appear collinear. The maximum spacing variation between A and B lines is 1.2  $\mu$ m.

tage of using resist and thin-film techniques is that they enable precise comparison of macroscopic and microscopic spatial-irradiance distributions.

In a subsequent section, photoresist methods are shown capable of determining the stepping precision of photorepeaters. Other types of measurements have been published elsewhere [15, 16].

### Lens evaluation

The objective of integrated-circuit mask technology is high-volume production of small images (e.g., lines and rectangles) having minimum dimensional errors of size and location over relatively large fields. This technology requires new types of lenses having performances unheard of a few years ago. The ideal test procedure for diffraction-limited lenses is one whose results can be directly applied to specify the fabrication process, which requires preservation of both macroscopic and microscopic dimensions. Lens distortion, as determined by macroscopic imaging measurements, is described first because of the simplicity of the corresponding test mask.

#### Macro-imaging

The photolithographic process permits direct measurement of distortion if targets are used in the form of parallel lines, as is shown in Fig. 1(a). The lens is mounted on the photorepeater and, after the first exposures of a resist-coated chrome plate, the stepping table moves the plate a distance equal to spacing  $S_0$ ; subsequently, a

second exposure is made. This procedure will result in an approximate superposition of the lines A and B of Fig. 1(a). More lines were used at B because the smallest unit of table displacement is equal to 25 µm, and it is desirable to have the image of line A in close proximity to one of the lines of set B. This procedure can be repeated for line pairs of various spacings, including center lines, as well as for different orientations. After completion of the exposures, the photoresist and chrome films are processed and the images evaluated by high-magnification photomicrography. Figure 1(b) shows distortion of the field of a diffraction-limited lens (F/1.8, f=50)mm, field diameter = 14 mm). Lines A and B can be easily distinguished by their different widths, and the line distances and spacing variation demonstrate barrel distortion.

This differential method, in combination with dark-field illumination photomicrography, permits distortion measurement with an accuracy of about  $0.03 \mu m$ .

The error-value judgement can be justified as follows. The bright lines that represent the edges of the chrome images under dark-field observation have a width of about  $0.5~\mu m$  in the object plane of a 0.95~N.A. objective. A reticle can be positioned symmetrically on a bright line with an error about ten times smaller than the line width [17]. Condenser adjustment and defocus are the primary sources of measurement error and cause deformations of the diffraction maxima that can be detected on the photomicrographs.

Distortion measurements having standard deviations better than 0.05  $\mu$ m are more than satisfactory, because present conventional projection equipment limits linewidths to about 2  $\mu$ m.

#### Micro-imaging

The next step is a study of the capability of a lens to produce small images of precise dimensions over the entire field of view. For this purpose, the photorepeater makes an effective test bench because of its stepping and adjustment capabilities and its stability. The input is an object in the form of a single segment of a chrome mask with lines, rectangles, squares, and other patterns of various sizes and orientations, in positive and negative form [10]. Typical targets are provided at the 10× size required for most repeater lenses and, therefore, can be measured with an accuracy that exceeds requirements by one order of magnitude. The various types of input patterns are reduced by the lens and recorded in positive photoresist, in which exposure and focus scan are variables. Such "dynamic" testing is recommended because it guarantees that at least one of the images coincides with or lies sufficiently close to the plane of best focus and is simultaneously recorded at optimum exposure. Determination of acceptable tolerances for the projec-

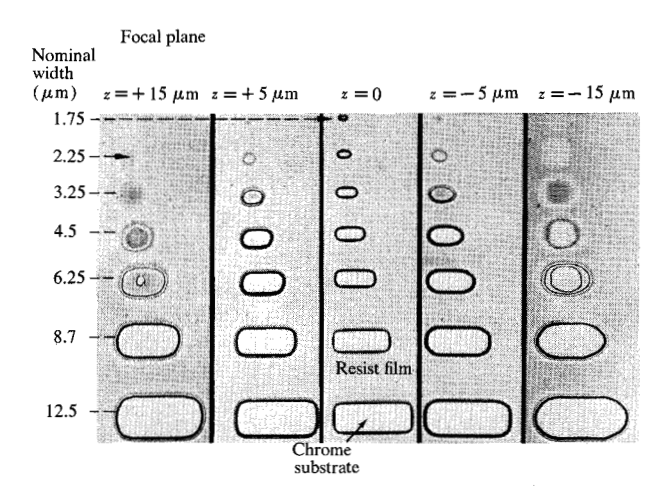


Figure 2 Rectangles of 3:1 ratio of length to width, exposed at constant times on positive resist at five different axial locations of the image plane. Deformation of the resulting images due to nonoptimum focus permits one to distinguish between exposure and defocus errors. (The interference fringes in the developed resist film indicate lines of equal irradiance and represent a third coordinate of measurement).

tion system, the plate waviness, and the resist thickness follow from the nature of images observed under nonoptimum conditions.

A typical tabular arrangement of the individual exposure and defocus steps of full-field images per plate may be made in the form that follows, all numerical quantities being relative:

State of focus*	Exposure time, percent					
in arbitrary units		75	85	100	115	135
Normalized depth of focus	+3 {+1 -1 -3		ita fo	r 20 st	epped	

<sup>\*</sup>Depth of focus = 2 units.

The total range of the focus scan should be about three to five times the depth of focus. The number of steps should never be less than nine, i.e., three exposure steps and three focusing steps for each exposure. The best images having optimized focus and exposure should be located near the center area of the stepped array. Sometimes data from one plate will suffice for all necessary information about a lens. Examination of the resist images in yellow light prior to etching is recommended because it will show quickly whether the test run is acceptable.

One problem is to differentiate between the effect of a small focus error [18] and a small exposure error, both of which affect linewidth. A good way to determine this is by observing the over-all shape of a small image, such

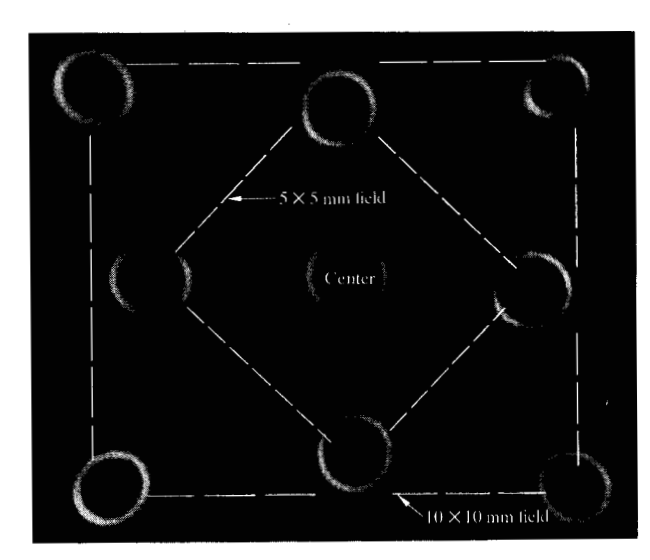


Figure 3 Dark-field images of 12.5- $\mu$ m squares of a  $50 \times 50$  mm field, reduced by a  $5 \times$  lens. After resist development and etching of the chrome film, the resulting images were magnified to  $1000 \times$ , photographed, and again magnified to  $8500 \times$ . The images in the four outer corners of the 10-mm square field appear radially elongated, which can be attributed to uncompensated off-axis aberrations. The ratio of the area of the largest image to that of the smallest is 1.5.

as a rectangle, because focusing error manifests itself independently of exposure variation by deformation of such images.

Figure 2 illustrates an example in which resist images on a chrome mask are used to evaluate effects of defocusing on a  $10\times$  reduction lens of F/1.8 and f=30 mm. The rectangular images of this lens tend to become ovals or ellipsoids if the image plane defocuses as it approaches the lens, but become somewhat sheared or rhomboid-like for loss of focus in the opposite direction. The resist images also give rise to interference fringes of equal thickness that, in turn, define areas of constant irradiance.

After the best focus is achieved, the ideal exposure time is ordinarily derived from a plot of exposure vs linewidth and is determined by equality of lines and spaces. Exposure tolerance can be determined from the same graph. The plate waviness tolerance can be determined in a similar fashion from a plot of the state of focus vs linewidth. In critical cases the combination of both tolerances must be taken into account.

After the focus and optimum exposure are established for one location within the field, the reproduction of images of the same size across the entire object plane must be evaluated. After resist exposure and development, the chrome substrate is etched. Chrome images are advantageous for planar measurements because the chrome film is thinner than 1000 Å.

Figure 3 shows the dark-field images of nominal 2.5  $\mu$ m squares which are obtained by a 5× reduction lens of F/1.8 and f=50 mm. The images cover a field of  $10 \times 10$  mm. Nine locations are shown: four in the corners, four more inside representing the four corners of a  $5 \times 5$  mm square, and one in the center.

For practical purposes, the image plane is placed so as to coincide with the plane of best focus.

Dark-field illumination is recommended for photomicrographic evaluation of thin film images, because image dimensions then do not depend on exposure time of the photomicrographs and a measuring reticle can be positioned symmetrically on the line edges, which appear as bright lines. Martin [19] has made some calculations which show that, under certain theoretical assumptions, the geometrical edges coincide with the center of the bright line images. The following user-related results that are observed are typical:

The images of the four outer corners of the  $10 \times 10$  mm field are slightly elongated in the radial direction, probably because of small, uncompensated aberrations.

In the four corners of the  $5 \times 5$  mm field, the images appear more symmetrical, i.e., they are rounded.

The ratio of the smallest area to the largest is about 1.5.

Image sizes vary along the periphery of the field because of small adjustment errors which, in addition to aberrations, are the primary cause of dimensional errors of the images.

Some remarks about measurement of small images are in order. Dimensional measurements of small images can be made by use of photoelectric microscopy, as studied by Dobrowalski et al. [20], Slater [21], Watrasiewicz [22], and others. However, this approach is not advisable because of the complexity and slowness of the measurement apparatus and the difficulty of measuring asymmetric images. Small spatial distributions have been measured with microdensitometers [23-25]. Generally, these systems are designed for measurement of silver halide emulsions, require relatively long slits, and are therefore even less suitable than the photoelectric system referenced above. In the present work a commercial microscope (N.A. = 0.95) with camera attachment is used. The photomicrographs are evaluated with a measuring loupe. This method reveals a maximum of information and is simple and inexpensive. A large number of authors have discussed accuracy of coincidence and symmetry settings, the impact of target lines with blurred edges, and related factors [26-31]. Michelson

[32] and Roblin [33] calculated and observed setting precisions smaller than 0.03  $\mu$ m.

The shapes and sizes of small images become increasingly important as integrated circuit components decrease in size. The following example demonstrates the changes of shape and total area of nominal  $2.5 \times 7.5~\mu m$  rectangles with changing exposures, in ratios of 0.6, 0.8, 1.1, and 1.5. After development and etching, the resulting chrome images are photographed under dark-field illumination. For precise tracing, a total magnification of  $8300\times$  is applied. The four chrome images which represent isophotes (contour lines of equal intensity) are superimposed in Fig. 4(a), displaying a section of the three-dimensional irradiance distribution. The dotted rectangle represents the ideal image of the object.

Another example shows that some causes of dimensional error (e.g., misalignment of the illumination system) can be detected without any dimensional measurement effort by taking advantage of the nonlinear relationship between exposure and the dimensions of small images; that is, by underexposing the positive photoresist so that only the peaks and top portions of the irradiance distributions are manifest on the resist film, Fig. 4(b). The spots of chrome film which were protected from etching by patches of resist appear black in transmitted-light photomicrography. The irradiance is strongest in the center of the field and decreases asymmetrically toward the outside, which indicates misalignment of the illuminator system.

## • Testing of macroscopic irradiance uniformity

A significant contribution to microscopic image variations is nonuniform macroscopic irradiance. It is possible to adopt a uniformity test as an integral part of the photolithographic process. To this purpose, a uniform film of positive resist is coated on a flat glass surface and various open-frame exposures of decreasing time are made. After development of the resist, any nonuniformity in the field will be manifest in a corresponding deviation from the average thickness of the residual resist film. This resist relief can easily be measured interferometrically. Fringe displacements of  $\lambda/20$  have been measured [34]. For a resist thickness of 1  $\mu$ m this corresponds to a precision of measurement of about two percent of the total required radiant flux for resist removal, which is satisfactory for photolithographic purposes.

Figure 5 shows an example of an interferogram of a gold-coated resist surface indicating a nonuniformity of about 20 percent, as verified by insertion of glass plates into a portion of the object plane, which introduces exposure steps of about eight percent. Resist thickness-to-exposure curves have also been measured by a number of authors [35-37]. Nonlinearity of the curve for resist

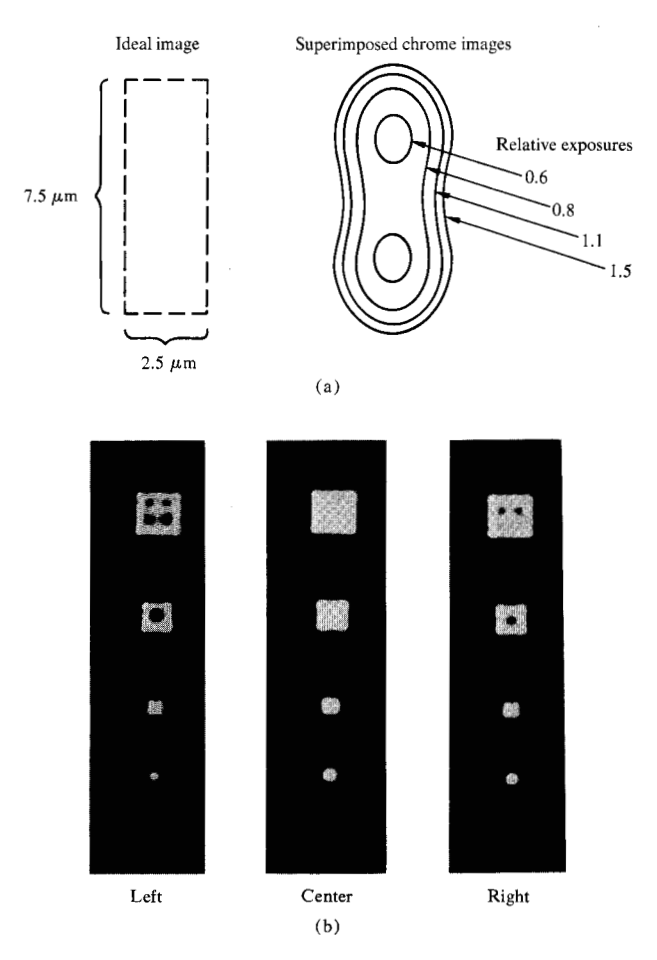


Figure 4 Irradiance distribution in micro-images. (a) Contour lines of equal irradiance of a nominal  $2.5 \times 7.5 \,\mu\mathrm{m}$  image in the plane of best focus ( $5\times$  reduction lens). The lines were traced from dark-field photomicrographs ( $8300\times$ ) of chrome images that represent four different exposures of positive photoresist. (b) Underexposed images are sensitive indicators of misalignment of the condenser or light source. One set of chrome images is located in the center and the other two at opposite ends of the field. Illuminator misalignment changes the irradiance distribution, causing image-size variations and asymmetric displacement of the residual chrome dots.

thickness vs exposure is of no concern, since only relatively small nonuniformities of irradiance are measured.

## Photorepeater stepping table

Some of the advantages that accrue from the symbiosis between thin film phototechnology and conventional microscopy were shown in the preceding sections. Previously the largest range of measurement was the field of a lens. In this section the precision of photorepeater stepping is determined and the practical limitations of the photolithographic process in terms of mask registration established.

229

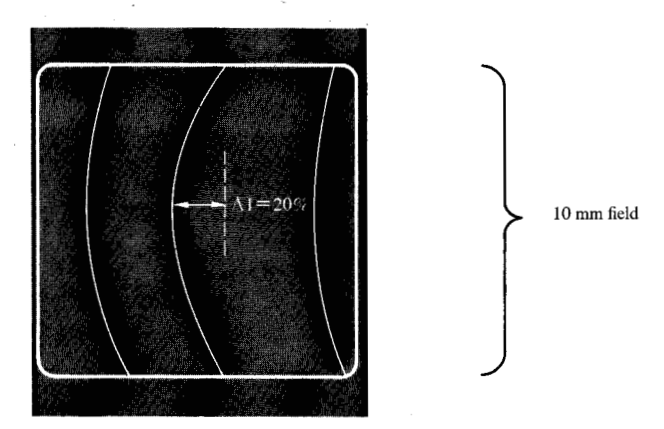
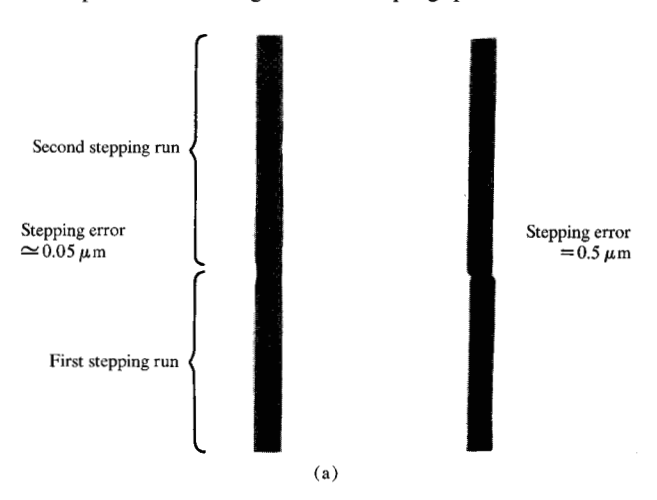
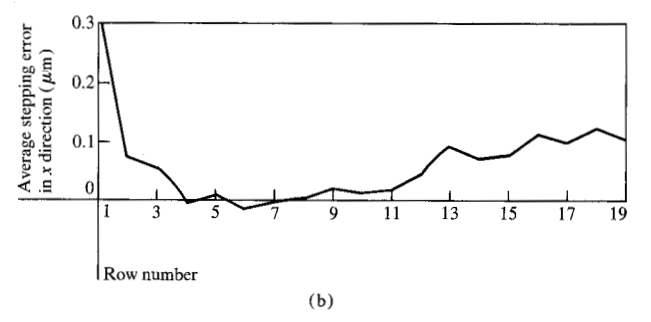


Figure 5 Determination of macroscopic irradiance distribution of a 5× lens. The partially exposed resist displays a concave surface (decreasing irradiance with increasing distance from the center of the field) which is sputter-coated with a thin film of gold and observed with a Fizeau interferometer. The nonuniformity of 20 percent is caused by a defective condenser system.

Figure 6 Photorepeater stepping error. (a) Two examples of short-term stepping error. Different portions of the same target line are stepped across the resist-coated chrome mask in subsequent stepping runs. The deviation from collinearity of the successively stepped lines is a measure of the stepping error. (b) Average short-term repeatability error in the x direction for 19 equally spaced rows of a  $70 \times 70$  mm field. The value for each row represents the average from 19 sampling spots.





Single lines perpendicular to the x and y direction of stepping serve as targets. For reasons of simplicity, stepping repeatability is demonstrated only in the x direction over a field of  $70 \times 70$  mm. Similar results have been obtained for the y direction.

A portion of the single-segment line is covered by an opaque mask, and a two-dimensional array is stepped onto a plate coated with a photosensitive film. After completion of the stepping operation, the machine is returned to its initial position. The opaque mask is placed in the complementary location so that the previously masked-off section of the line can be exposed while the exposed section is covered by the mask. A second stepping operation is performed; more can be added if desired. After processing the resist and etching the chromium, the short-term repeatability is determined with a measuring microscope.

If the precision of the machine is perfect, the microscopic observation shows only straight lines. Lack of repeatability of the machine degrades the coincidence of the collinear, and sequentially stepped, line pairs to a greater or lesser degree, as shown in Fig. 6(a). The precision can also be measured by small parallel displacements of the segment between repetitive runs.

The short-term repeatability was measured at 361 sampling points which were uniformly distributed over the 70 mm  $\times$  70 mm field. Figure 6(b) gives the average precision per row.

The following conclusions can be drawn from the data:

- The first row shows up worst since it takes time to establish dynamic equilibrium. The average repeatability error is 0.3 μm. In production, no exposures are made until dynamic equilibrium is achieved.
- The first and last rows are worse than those in the middle; this indicates a systematic error, probably due to slight tilting of the stages.
- 3. Eight rows show an average short-term repeatability error of less than  $0.05 \mu m$ .
- 4. The standard deviation  $\sigma$  of the stepping precision is about 0.1  $\mu$ m.

These results, which present the stepping capabilities of photorepeaters made since the late 1960s, demonstrate that their limitations of precision are responsible for the smallest mask registration error in the photolithographic portion of integrated circuit fabrication.

Registration errors between the masks of a set which are introduced during wafer-to-mask alignment and contact printing are generally multiples of the photorepeater precision. Therefore, it appears useful to denote the conventional  $3\sigma$  value for the stepping precision, i.e., 0.3  $\mu$ m, as the present "practical limit" of photolithographic technology.

Future advances can be considered along the following lines. First, dimensional errors that are caused, for instance, by wafer-to-mask alignment and contact printing should be reduced at least to  $0.3~\mu m$ . Second, the tolerances of other quantities that affect mask registration (e.g., magnification and exposure error, mask and wafer flatness) should be reduced to the  $0.3~\mu m$  practical limit mentioned above. Third, improvement of photorepeater stepping would be warranted only after this dimensional tolerance limit is achieved for all variables that contribute significant errors. The degree of improvement obtained in stepping precision depends on the minimum image size that can be produced in high-volume fabrication.

#### Acknowledgment

I thank A. G. Lemke for his encouragement and for support of this project.

#### References

- K. Murata, Progress in Optics V, John Wiley and Sons, Inc., New York, 1965, p. 201.
- 2. R. R. Shannon, Optical Instruments and Techniques, Oriel Press Limited, London, 1970, p. 331.
- 3. R. E. Hopkins and D. Dutton, Opt. Acta 18, 105 (1971).
- R. V. Shack, U.S. National Bureau of Standards Circular No. 526, 1954, p. 275.
- 5. F. G. Back, J. Opt. Soc. Am. 43, 685 (1953).
- H. B. Hammill and T. M. Halladay, SPIE Journal 8, 223 (1970).
- 7. C. P. Bray, Appl. Opt. 11, 58 (1972).
- 8. Symposium on Astronomical Optics and Related Subjects (1955), Ed., Z. Kopal, Interscience Publishers, New York, 1956, p. 61.
- F. E. Washer and I. C. Gardner, U.S. National Bureau of Standards Circular No. 533, 1953.
- H. R. Rottmann, Proceedings of the INTERFACE '72 Microelectronics Seminar, Kodak Publication No. P-312.
- 11. A. A. Magill, J. Opt. Soc. Am. 45, 148 (1955).
- 12. A. H. Bennet, J. Opt. Soc. Am. 14, 235 (1927).

- 13. J. Zimmerman, Appl. Opt. 2, 759 (1963).
- 14. J. Hohenstein, Rev. Sci. Instr. 37, 1007 (1966).
- 15. F. T. Klostermann Philips Tech. Rev. 30, No. 3, 64 (1969).
- 16. D. S. Alles et al., Bell System Tech. J. 49, 2145 (1970).
- R. Schulze, Encyclopedia of Physics, Ed., S. Flügge, Springer Verlag, Berlin, Heidelberg, and New York, Vol. 29, 1967, p. 764.
- 18. P. E. Stokseth, J. Opt. Soc. Am. 59, 1314 (1969).
- 19. L. C. Martin, Proc. Phys. Soc. (London) 55, 104 (1943).
- J. A. Dobrowalski, W. Godfrey, P. N. Slater and W. Weinstein, J. Opt. Soc. Am. 47, 186 (1957).
- 21. P. N. Slater, J. Opt. Soc. Am. 49, 562 (1959).
- 22. B. M. Watrasiewicz, Opt. Acta 13, 167 (1965).
- 23. R. E. Kinzly, J. Opt. Soc. Am. 62, 386 (1972).
- 24. W. Czepluch, Optik 34, 432 (1972).
- K. Bonse, E. Kappler, and E. Simon, Angew. Phys. 16, 292 (1963).
- 26. A. H. Cook, Proc. Roy. Soc. (London) 219A, 500 (1955).
- 27. H. Hartridge, Phil. Mag. Ser. 6, 46, No. 271, 49 (1923).
- 28. J. Guild, Trans. Opt. Soc. 31, 1 (1929-30).
- R. T. Leslie and I. D. Armstrong, Australian J. Appl. Sci. 6, 168 (1955).
- 30. Yves Le Grand, Form and Space Vision, Indiana University Press, Bloomington, Ind., and London, 1969.
- 31. G. Foerster, Optik 2, 32 (1946).
- 32. A. A. Michelson, J. Opt. Soc. Am. and Rev. Sci. Instr. 8, 321 (1924).
- 33. G. Roblin, Opt. Acta 17, No. 13, 189 (1970).
- E. Lau and W. Krug, Equidensitometry, Focal Press, New York, 1968.
- 35. J. P. Kirk and G. L. Fillmore, Appl. Opt. 10, 2347 (1972).
- M. J. Beesley and J. G. Castledine, Appl. Opt. 9, 2720 (1970).
- 37. R. G. Brandes and R. K. Curran, Appl. Opt. 10, 2101 (1971).

Received April 16, 1973.

The author is located at the IBM System Products Division Laboratory, East Fishkill (Hopewell Junction), New York 12533.